PCCP

RSC Publishing

PAPER

View Article Online
View Journal | View Issue

Cite this: *Phys. Chem. Chem. Phys.*, 2013, **15**, 7666

Two-photon absorption spectra of a near-infrared 2-azaazulene polymethine dye: solvation and ground-state symmetry breaking†

Honghua Hu,[a] Olga V. Przhonska,[ab] Francesca Terenziani,[c] Anna Painelli,[c] Dmitry Fishman,[a] Trenton R. Ensley,[a] Matthew Reichert,[a] Scott Webster,[a] Julia L. Bricks,[d] Alexey D. Kachkovski,[d] David J. Hagan[ae] and Eric W. Van Stryland*[ae]

Received 22nd February 2013,
Accepted 19th March 2013

DOI: 10.1039/c3cp50811k

www.rsc.org/pccp

Polymethine dyes (PDs) with absorption bands in the near-infrared region undergo symmetry breaking in polar solvents. To investigate how symmetry breaking affects nonlinear optical responses of PDs, an extensive and challenging experimental characterization of a cationic 2-azaazulene polymethine dye, including linear absorption, fluorescence, two-photon absorption and excited-state absorption, has been performed in two solvents with different polarity. Based on this extensive set of experimental data, a three-electronic-state model, accounting for the coupling of electronic degrees of freedom to molecular vibrations and polar solvation, has been reliably parameterized and validated for this dye, fully rationalizing optical spectra in terms of spectral position, intensities and bandshapes. In low-polarity solvents where the dye is mainly in its symmetric form, a nominally forbidden two-photon absorption band is observed, due to a vibronic activation mechanism. Inhomogeneous broadening plays a major role in polar solvents: absorption spectra represent the weighted sum of contributions from states with a variable amount of symmetry breaking, leading to a complex evolution of linear and nonlinear optical spectra with solvent polarity. In more polar solvents, the dominant role of the asymmetric form leads to the activation of two-photon absorption as a result of the symmetry lowering. The subtle interplay between the two mechanisms for two-photon absorption activation, vibronic coupling and polar solvation, can be fully accounted for within the proposed microscopic model allowing a detailed interpretation of the optical spectra of PDs.

1. Introduction

Development of novel nonlinear optical (NLO) organic materials is important for many applications including multi-photon imaging, optical telecommunications, and all-optical switching.[1–6] Structure–property relations for many classes of organic molecules are already established, allowing the understanding of the main linear and NLO properties of existing compounds, and helping in the design of new molecules with optimized properties.[1,2,7–10] A strategy for enhancing the two-photon absorption (2PA) cross section (δ_{2PA}) of organic chromophores involves the increase of the ground-to-excited state transition dipole moment, μ_{01}, which in polymethine dyes can be achieved by lengthening the π-conjugated framework, either by lengthening the main chain,[2] or by extending the π-conjugation into the end groups.[3] For linear conjugated molecules, the molar absorptivity, ε, can be as large as 100 000–300 000 M^{-1} cm^{-1}, which corresponds to μ_{01} in the range of 12–18 D. However, for long molecules absorbing in the near-infrared (NIR) region around 1000 nm, μ_{01} values saturate due to the occurrence of symmetry breaking in the ground state. The effects of symmetry breaking on linear and NLO properties of polymethine dyes have already been discussed with reference to two families of polymethine dyes,[3,11,12] and more recently the effects of counter ions and

[a] *CREOL & FPCE, The College of Optics and Photonics, University of Central Florida, Orlando, FL 32816, USA. E-mail: ewvs@creol.ucf.edu*
[b] *Institute of Physics, National Academy of Sciences, Prospect Nauki 46, Kiev, 03028, Ukraine*
[c] *Dipartimento di Chimica and INSTM UdR-Parma, Università di Parma, Parco Area delle Scienze 17/a, 43124 Parma, Italy*
[d] *Institute of Organic Chemistry, National Academy of Sciences, Murmanskaya 5, Kiev, 03094, Ukraine*
[e] *Department of Physics, University of Central Florida, Orlando, FL 32816, USA*

† Electronic supplementary information (ESI) available: Additional characterization and experimental data (Fig. S1–S4), derivation of mathematical equivalence between dimerization model and ion pair model, details of experimental procedures for 2PA study. See DOI: 10.1039/c3cp50811k

aggregation have been also considered.[5] In this paper, we undertake an extensive and challenging study of optical spectra, including linear absorption, fluorescence, 2PA and excited-state absorption (ESA), of a cationic 2-azaazulene polymethine dye absorbing in the NIR, dissolved in two solvents of different polarity. This dye, despite being charged, has the interesting characteristic of being soluble in high- to medium-polarity solvents, so that the spectroscopic effects of solvation on the symmetry-breaking behavior can be investigated.

In particular, we demonstrate that this dye does not undergo symmetry breaking in low-polarity solvents, while it is preferentially in a broken-symmetry ground state when dissolved in high-polarity solvents. The experimental observation of a quite different shape and intensity of the 2PA response of the 2-azaazulene polymethine dye according to the solvent polarity is interpreted and reproduced based on the essential-state modelling, as due to the complex interplay between inhomogeneous broadening, vibronic and symmetry-lowering effects.

2. Experimental methods and results

We report the one-photon absorption (1PA), 2PA and ESA spectra of the NIR polymethine dye, 2-butyl-6-[7-(2-butyl-1,3-dimethylcyclo-hepta[*c*]pyrrol-6(2*H*)-ylidene)hepta-1,3,5-trien-1-yl]-1,3-dimethylcyclohepta[*c*]pyrrolium tetrafluoroborate, referred to as JB17-08 (see Fig. 1), in two solvents of different polarity: dichloromethane (DCM) and acetonitrile (ACN). The solvent polarity, measured by $\Delta f = (\varepsilon - 1)/(2\varepsilon + 1) - (n^2 - 1)/(2n^2 + 1)$ (ε and n are the solvent dielectric constant and refractive index, respectively), increases from 0.217 for DCM to 0.306 for ACN.[13] This is the largest Δf difference we can use, since JB17-08, a cationic dye, is poorly soluble in solvents less polar than DCM.

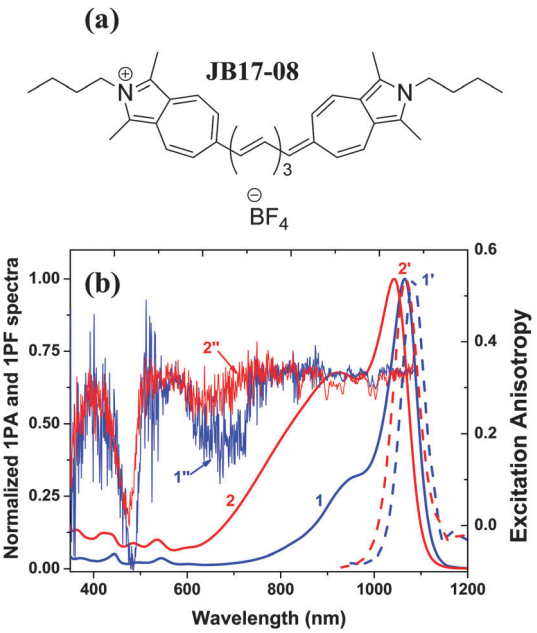

Fig. 1 (a) Molecular structure; (b) 1PA (1, 2), 1PF (1′, 2′) and excitation anisotropy (1″, 2″) spectra of JB17-08 in DCM (1, 1′, 1″), and ACN (2, 2′, 2″). Note that the 1PA spectra are recorded at concentrations where aggregation is virtually zero; detailed study of aggregation is described in Section 2.2.

2.1. Linear characterization

The 1PA (recorded by a Varian Cary 500 spectrophotometer), fluorescence (1PF) and excitation anisotropy spectra (measured by a PTI QuantaMaster spectrofluorometer) of JB17-08 are shown in Fig. 1. Despite the relatively short conjugation length of the molecule ($n = 3$), the linear absorption peaks are located at ~1000 nm due to extensive delocalization of charge in the end groups, equivalent to the extension of the polymethine chain to approximately 3 vinylene groups.[14] Increasing solvent polarity from DCM to ACN leads to a substantial broadening of the 1PA spectrum with the growth of a short-wavelength shoulder. This effect is typical for charged linear conjugated molecules (either cationic, or anionic)[11] absorbing in the range around 1000 nm and undergoing symmetry breaking. Broken-symmetry ground states, also called asymmetric forms, show an asymmetric charge distribution, a large bond-length alternation and hence a blue-shifted absorption.[12] The phenomenon of symmetry breaking has been discussed in terms of charge density waves (or solitonic waves) in linear conjugated chromophores,[12,15] and has been generalized to the family of quadrupolar dyes with a large permanent quadrupolar moment.[11,16]

The fluorescence spectra of JB17-08 in DCM and ACN, corrected for the spectral responsivity of the detection system, are characterized by a narrow band in both solvents, confirming that emission comes from a symmetric form with almost equalized bond lengths along the polymethine chain, in agreement with results obtained for other dyes with a broken-symmetry ground state.[11,17] The fluorescence quantum yield, Φ, is measured with reference to a photochemically stable cationic polymethine dye 3-ethyl-2-[7-(3-ethyl-1,1-dimethyl-1,3-dihydro-2*H*-benzo[*e*]indol-2-ylidene)hepta-1,3,5-trienyl]-1,1-imethyl-1*H*-benzo[*e*]indolium-4-methylbenzenesulfonate (labeled as PD2631) with $\Phi = 0.11 \pm 0.01$, recently proposed as a fluorescence standard near 800 nm.[17] The fluorescence quantum yield of JB17-08 is small, $\Phi \approx 0.05$, in both solvents, in line with the comparatively short fluorescence lifetime, $\tau_F = 28.5 \pm 2$ ps, measured by a pump–probe technique[2,18] (see Section 2.3.2). The lifetime is short compared to the orientational motion of the solute in ACN and DCM (typical values are 350–450 ps),[18] allowing for the measurement of fluorescence anisotropy spectra in these low-viscosity solvents. The excitation anisotropy spectrum, $r(\lambda)$, measured at a fixed emission wavelength corresponding to the maximum of the fluorescence band, is defined as: $r(\lambda) = [I_{\parallel}(\lambda) - I_{\perp}(\lambda)]/[I_{\parallel}(\lambda) + 2I_{\perp}(\lambda)]$ where $I_{\parallel}(\lambda)$ and $I_{\perp}(\lambda)$ are the intensities of the fluorescence signal polarized parallel and perpendicular to the excitation light, respectively.[13] The excitation anisotropy spectra in DCM and ACN (shown in Fig. 1b) are somewhat noisy due to the weak fluorescence quantum yield ($\Phi \approx 0.05$). In any case, both anisotropy spectra show similar trends: they are flat within the main absorption band (up to ~750 nm) with $r(\lambda) \approx 0.35$, indicating almost

aligned transition dipole moments for the absorption and emission processes. The decrease in the $r(\lambda)$ value in the 700–550 nm spectral range locates the position of the next electronic state (or group of states) with an angle of $\sim 30^\circ$ between the absorption and emission dipoles. The deepest valley is observed in the range 430–470 nm, indicating an angle up to 65° between the two transition dipoles. Magnitudes of anisotropy valleys in ACN are somewhat smaller, which could indicate the influence of the asymmetric form with a slightly different orientation of the transition dipole moments.

The $S_0 \rightarrow S_1$ transition dipole moment can be estimated from the area beneath the main linear absorption band as (SI units but where otherwise specified):[13]

$$\mu_{01} = \sqrt{\frac{3 \ln 10 \hbar c \varepsilon_0}{10\pi N_A \tilde{\nu}_{01}} \int \varepsilon_{01}(\tilde{\nu}) \mathrm{d}\tilde{\nu}} \qquad (1)$$

where $\hbar$ is the Planck constant divided by 2π, c is the speed of light, ε_0 is the vacuum permittivity, N_A is Avogadro's number, $\varepsilon_{01}(\tilde{\nu})$ is the molar extinction coefficient (expressed in $cm^{-1}\ M^{-1}$), $\tilde{\nu}_{01}$ is the transition wavenumber (in cm^{-1}) at the maximum of absorption, and the integral is performed over the main absorption band ($\tilde{\nu}$ in cm^{-1}). Based on eqn (1), $\mu_{01} \approx 18$ D in both DCM and ACN solutions.

2.2. Aggregation study

Polymethine dyes, due to their large polarizabilities, easily aggregate at the high concentrations required for NLO studies.[5,19] Since molecular aggregates not only hinder the accurate determination of the monomer concentration in solution, but also may influence linear and nonlinear optical properties, we perform a concentration-dependent linear absorption analysis of JB17-08 in DCM and ACN. The concentration of dye molecules varies in the range between 10^{-3} M, close to saturation, to 10^{-6} M where aggregation is absent as verified by further dilution. Correspondingly, the cell path lengths range from 100 μm to 1 cm. The absorption spectrum can in general contain contributions from both monomer and aggregated species. Here we define the apparent molar absorptivity, $\varepsilon_A = A/(LC_0)$, where A is the absorbance (*i.e.* optical density) of the solution; L is the cell path length and C_0 is the *total* (nominal) concentration of the dye in solution.

The apparent molar absorptivity spectra $\varepsilon_A(\lambda)$ for JB17-08 in DCM are shown in Fig. 2a, with the total dye concentrations ranging from 3.4 mM down to 3.5 μM. At the highest concentration (3.4 mM) a flat plateau is observed in the absorption spectra in the 1025–1090 nm region due to the extremely low transmittance of the solution ($A > 3.5$), beyond the measurement capability of the spectrophotometer. Decreasing the concentration below 0.042 mM does not significantly alter the spectra, indicating the absence of aggregates below this concentration (spectra are not shown because they are superimposed on curve 4). A well-defined isosbestic point is observed at ~900 nm, pointing to a well-defined equilibrium between two species in solution. The two species can correspond to monomer (M) and dimer (D), and the relevant equilibrium

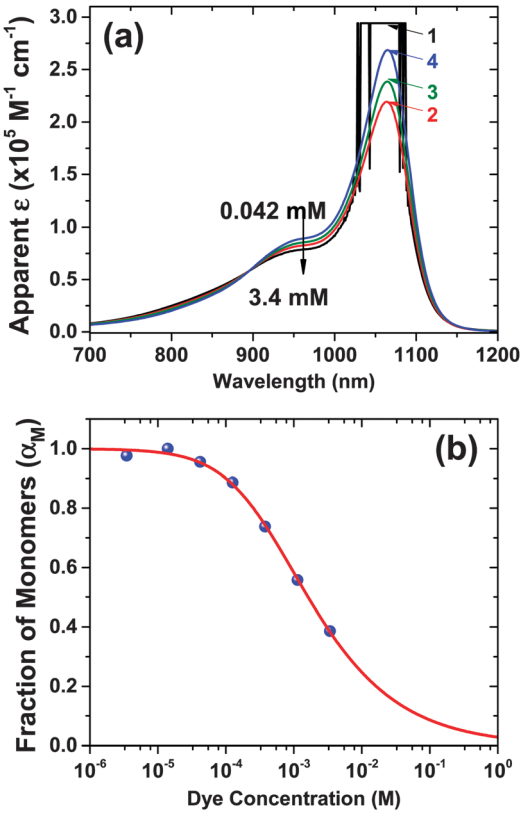

Fig. 2 JB17-08 in DCM: (a) apparent absorptivity spectra $\varepsilon_A(\lambda)$ measured at concentrations 3.4 mM (1), 1.1 mM (2), 0.38 mM (3), and 0.042 mM or lower (4); (b) the fraction of monomers (α_M) at different total dye concentrations (C_0), calculated based on the apparent ε_A and absorptivity of dimers $\varepsilon_D = 0.58 \times 105\ M^{-1}\ cm^{-1}$ at 1100 nm using eqn (4) (blue dots), and the fitting, calculated from eqn (3) (red curve).

2M ↔ D (referred to as a dimerization process) will be described here according to the procedure discussed by Würthner *et al.*[20] Alternatively, the equilibrium could be ascribed to the incomplete dissociation of the molecule to a cationic part and its counter-ion resulting in the formation of cation–counter-ion complexes.[5] As it will be discussed later, this type of process would lead to similar conclusions as for dimerization.

According to the dimerization model, the concentrations of dimers and monomers, C_D and C_M, respectively, are connected by:

$$K_D = \frac{C_D}{C_M^2} = \frac{1 - \alpha_M}{2\alpha_M^2 C_0} \qquad (2)$$

where K_D is the dimerization constant for the 2M ↔ D equilibrium, and $\alpha_M = C_M/C_0$ is the fraction of monomers in the solution. Solving eqn (2) for α_M we obtain:

$$\alpha_M = \frac{\sqrt{8K_D C_0 + 1} - 1}{4K_D C_0} \qquad (3)$$

The apparent molar absorptivity, ε_A, can be expressed as:

$$\varepsilon_A = \alpha_M \varepsilon_M + (1 - \alpha_M)\varepsilon_D \qquad (4)$$

where ε_M and ε_D are the molar absorptivity of monomer and dimer, respectively. Combining eqn (3) and (4), leads to:

$$\varepsilon_A = \frac{\sqrt{8K_D C_0 + 1} - 1}{4K_D C_0}(\varepsilon_M - \varepsilon_D) + \varepsilon_D \qquad (5)$$

A nonlinear regression (see ESI,† Fig. S1) of the C_0-dependence of the apparent ε_A measured at 1100 nm leads to K_D = 616 L mol^{-1}, and $\varepsilon_D = 0.58 \times 10^5$ M^{-1} cm^{-1} at 1100 nm. Note that in the fitting procedure we fixed ε_M (at 1100 nm) = 1.1×10^5 M^{-1} cm^{-1}, as determined from optical spectra collected from an extremely dilute solution (3.5 μM). We also use a similar procedure to fit the apparent ε_A at 1064 nm and 775 nm, as shown in Fig. S1 in ESI.† All fittings give the same K_D within a 10% uncertainty. Based on this analysis, the monomer fraction (α_M) is estimated as a function of the nominal dye concentration C_0, as shown in Fig. 2b. At concentrations larger than 0.25 mM, the dimer fraction becomes significant, with $\alpha_M < 0.8$. Based on the $\varepsilon_A(\lambda)$ spectrum measured at 1.1 mM, characterized by a large dimer fraction (α_M = 0.56), and at 3.5 μM (essentially corresponding to the pure monomer, *i.e.* $\alpha_M > 0.99$), eqn (4) allows us to extract the linear absorption spectrum of the dimer, as shown in Fig. 3a. The peak of the dimer absorption nearly coincides with the absorption peak of the monomer, but it is broader in the short-wavelength range. The reconstructed absorptivity spectra at 3.4 mM (α_M = 0.38) and 0.4 mM (α_M = 0.74) is in excellent agreement with the experimental spectra, as shown in Fig. S2 in ESI.†

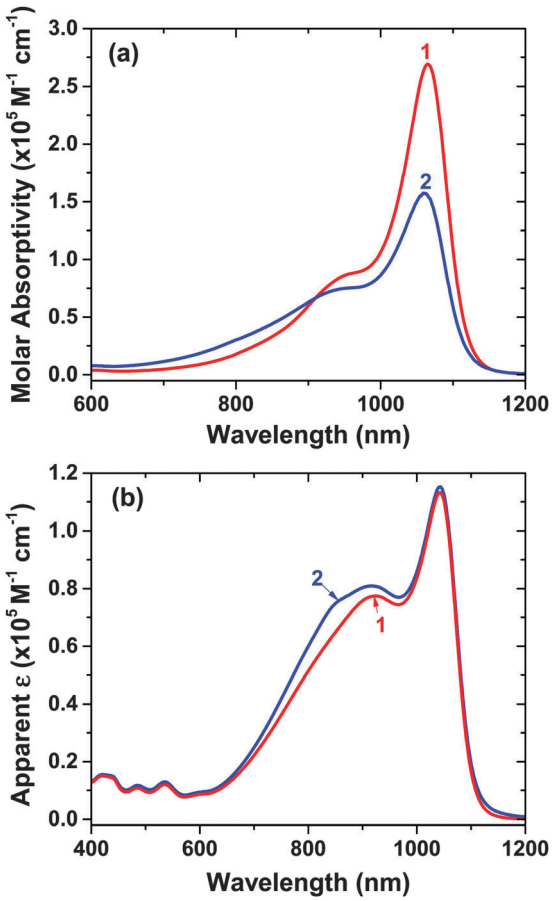

Fig. 3 (a) JB17-08 in DCM: the absorptivity spectrum $\varepsilon_A(\lambda)$ at a concentration of 3.5 μM ($\alpha_M > 0.99$, *i.e.* basically the monomer spectrum) (1), and the absorptivity spectrum of the dimer (2) extracted by the use of eqn (4); (b) JB17-08 in ACN: the absorptivity spectra $\varepsilon_A(\lambda)$ measured at 14 μM (1), and 1.4 mM (2).

As mentioned above, the equilibrium, evidenced by the spectra in Fig. 2a, could be ascribed to an incomplete dissociation of the cationic dye from its counter-ion in the low-polarity solvent DCM. As discussed in the ESI,† the relevant equilibrium (cation + counter-ion ↔ ion pair) can be described using the same mathematical expressions used for the dimerization model, leading to the same relation between the fraction of cation and the total dye concentration as reported in Fig. 2b, with the absorption spectrum of the ion pair corresponding to curve 2 of Fig. 3a. In the lack of additional information we cannot distinguish between the two mechanisms, and we can only state that in concentrated DCM solutions an aggregate species (either a dimer or an anion–cation pair) is found, whose concentration and spectrum can be extracted from the careful analysis of experimental data.

Similar concentration-dependent analyses of linear absorption spectra are performed for JB17-08 in ACN at concentrations ranging from 1.4 mM to 14 μM, as shown in Fig. 3b. Small spectral changes between the high and low concentrations are observed around 840 nm, while the peak molar absorptivity at 1043 nm changes less than 5%. Further dilution below 14 μM does not lead to any change of the spectral shape. Therefore, we conclude that the aggregation of JB17-08 in the polar ACN solution is not significant up to 1.4 mM.

2.3. Nonlinear characterization

2.3.1. 2PA spectra: results and analysis. Frequency-degenerate 2PA spectra of JB17-08 in DCM and ACN are measured by the open-aperture Z-scan technique[21] using femtosecond laser pulses. With this technique, the 2PA cross section, δ_{2PA}, is directly obtained without the need for 2PA references. Tunable femtosecond excitation pulses (from 300 to 2600 nm) are generated by an optical parametric generator/amplifier (OPG/OPA, Light Conversion Ltd. model TOPAS-800) pumped by a regenerative Ti:Sapphire amplifier (Clark-MXR operating at a 1 kHz repetition rate). Pulsewidths (<150 fs, FWHM) are measured independently by the second-harmonic autocorrelation technique. To verify the spot size of the beam at the focus, we also performed Z-scans on the semiconductor GaAs and fit the data with known parameters.[22] Both DCM and ACN solvents show significant linear absorption in the wavelength range of interest (1300–2100 nm), and their linear absorption is taken into account in the fitting procedure adopted to analyze δ_{2PA}. Nonlinear absorption from the solvents was measured separately and not detected.

As discussed in Section 2.2, the significant aggregation (either dimerization or ion-pair formation) of JB17-08 in DCM complicates the analysis. To safely exclude significant 2PA contribution from aggregates, concentrations less than 0.1 mM (*i.e.* $\alpha_M > 0.9$, see Fig. 2b) are needed. However, at these low concentrations the determination of the complete 2PA spectrum

is very difficult, given that the open-aperture Z-scan signals (from 2PA), measured at pulse energies below the damage threshold, are weak against the noise level of the detection system. Therefore, in order to obtain a relatively accurate *shape* of the δ_{2PA} spectrum of JB17-08 in DCM, we performed Z-scan measurements at a concentration of 3 mM, despite the fact that the monomer fraction at this concentration is only 0.4. However, at several wavelengths between 1550 and 1800 nm, where the δ_{2PA} is relatively large, we performed dual-arm Z-scans (DA Z-scan)[23] on a series of solutions with C_0 ranging from 5 mM down to 0.1 mM to study the effect of aggregation on the 2PA of the solution and determine the δ_{2PA} of the monomer. Additionally we use two-photon fluorescence (2PF) to determine the δ_{2PA} of the monomer in a 0.1 mM solution at 1850 nm and 1900 nm. Details of the experiments are discussed in the ESI.†

The δ_{2PA} spectrum of JB17-08 in DCM, measured in the 3 mM solution and rescaled to the δ_{2PA} of the monomer measured at 0.1 mM at several wavelengths, is shown in Fig. 4. Note that the measured data are reproducible, including the dip observed between 1800 nm and 2000 nm (absolute experimental error is ±25%). The apparent δ_{2PA}, measured at different dye concentrations from 5 mM to 0.1 mM for several wavelengths between 1550 and 1800 nm, is shown in Fig. 5 as a function of the estimated monomer fraction in solution. The apparent δ_{2PA}, analogously to the apparent linear absorptivity ε_A, discussed in Section 2.2, is calculated based on the C_0 of the solution. To demonstrate the signal-to-noise level of our detection system, we include Z-scan traces at 1550 nm and 1800 nm for the 0.1 mM solution in Fig. S3 in the ESI.† We also include in Fig. S4 (ESI†) the 2PF signal for the 0.1 mM solution excited at 1800 nm, 1850 nm and 1900 nm under the same excitation irradiance: δ_{2PA} at 1850 nm and 1900 nm are determined scaling to the integrated area of the 2PF signal excited at 1800 nm. As seen from Fig. 5, the apparent δ_{2PA} is maximum

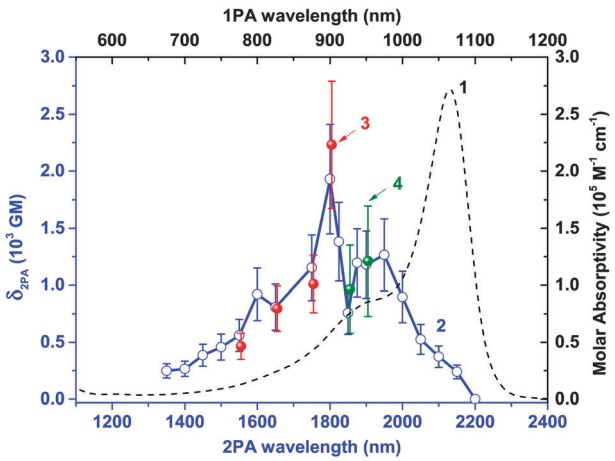

Fig. 4 JB17-08 in DCM. Molar absorptivity spectrum (1, dash curve) at 3.5 μM (α_M > 0.99), 2PA spectrum (2, open circle + solid blue curve) measured at 3 mM and rescaled to the δ_{2PA} values obtained at 0.1 mM by Z-scan (3, red solid dots) and by 2PF (4, green solid dots) techniques; as described in Section 2.3.1, curve 2 represents the 2PA spectrum of the monomer molecules in DCM solution.

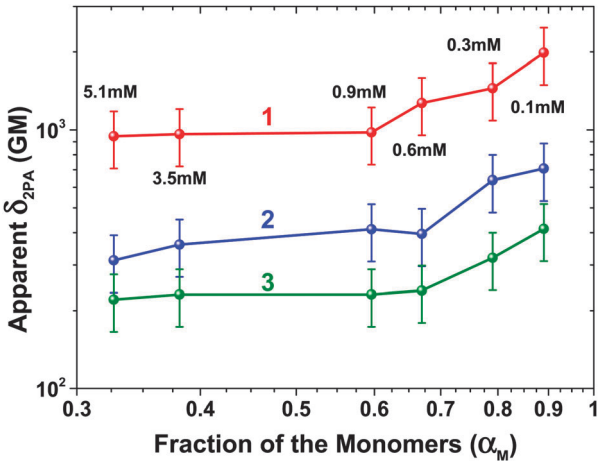

Fig. 5 log–log plot of the apparent δ_{2PA} values of JB17-08 in DCM solution *vs.* the fraction of monomer molecules α_M, measured at wavelengths 1800 nm (1), 1650 nm (2) and 1550 nm (3). The corresponding dye concentrations vary from 5.1 mM to 0.1 mM. Solid curves are guides to the eye.

for the smallest concentration measured, 0.1 mM, followed by a steady decrease at larger dye concentrations corresponding to a decrease of the fraction of monomers α_M. This trend, quite independent of wavelength, is a clear indication that the 2PA contribution from aggregated dye molecules is significantly less than the 2PA from the monomer molecules. Therefore, at a concentration of 0.1 mM, where the fraction of monomers is 0.9, we can estimate the δ_{2PA} of monomers by dividing the apparent δ_{2PA} by α_M, as shown by the red solid data points in Fig. 4. However, as the dye concentration increases beyond 0.9 mM, the apparent δ_{2PA} reaches more or less a constant value (approximately half of that obtained at 0.1 mM), suggesting a significant influence from aggregates beyond 0.9 mM. The estimation of δ_{2PA} from the aggregates (either dimers or cation–counter-ion complexes) is not straightforward.[5] Nevertheless, it is very important that the *spectral shape* of the δ_{2PA} spectrum from monomer species (at a concentration of 0.1 mM, measured by either Z-scan or 2PF techniques) closely follows the spectral shape measured at 3 mM, as shown in Fig. 4. These results verify our assumption that the δ_{2PA} measured at 3 mM approximates well the δ_{2PA} spectrum of the JB17-08 monomer in DCM solution.

As discussed in Section 2.1, the one-photon $S_0 \rightarrow S_1$ absorption band in DCM shows a dominant contribution from the symmetric form of the dye, for which a direct $S_0 \rightarrow S_1$ 2PA transition is forbidden by symmetry. Therefore, the main channel for the observed 2PA intensity in the $S_0 \rightarrow S_1$ spectral range for DCM solutions can be attributed to electron-vibration coupling.[24] Accordingly, the peak of the experimental 2PA spectrum in DCM is blue-shifted, with its 2PA final states located on the vibronic shoulder of the 1PA peak. The structure of the 2PA band is fairly complex, suggesting the possible involvement of several vibrational modes. There are two clearly distinguishable peaks and a tentative possible third peak in the 2PA spectrum of JB17-08 in DCM: one roughly corresponds to a vibrational shoulder in the 1PA band (skeleton vibration of ~1200 cm^{-1}), which is typical

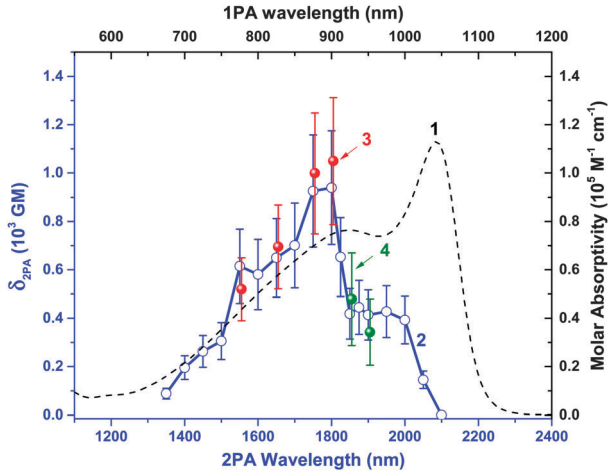

Fig. 6 JB17-08 in ACN. Molar absorptivity spectrum (dash curve 1) at 6.6 μM, 2PA spectrum at 1.3 mM (blue open dots + blue solid curve 2) in comparison with the δ_{2PA} values measured at a concentration of 0.18 mM by Z-scan (3, red solid dots) and at 0.07 mM by 2PF (4, green sold dots).

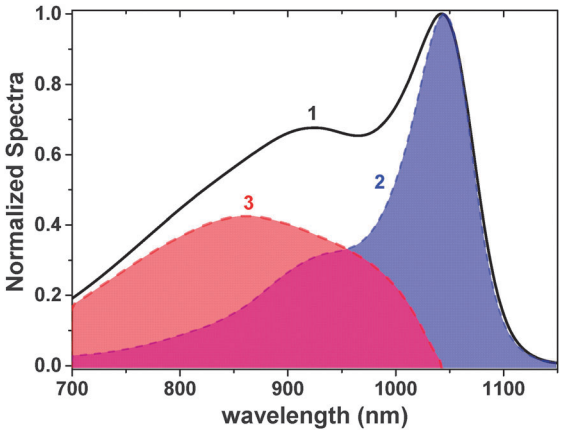

Fig. 7 JB17-08 in ACN: linear absorption spectrum (1); contribution of the symmetric form (blue shaded area, ~42%) (2); contribution of the asymmetric form (red shaded area, ~58%) (3).

for polymethine molecules, and the additional peak (or possibly two) corresponding to vibrational modes around 800 cm^{-1} not resolved in the 1PA spectrum.

The δ_{2PA} spectrum of JB17-08 in ACN solution, measured at a concentration of 1.3 mM is shown in Fig. 6. Since, as discussed in Section 2.2, the aggregation of JB17-08 in ACN is relatively minor, δ_{2PA} values are estimated neglecting any aggregation effect. However, δ_{2PA} was measured at several wavelengths for ACN solutions of JB17-08 at concentration 0.18 mM by DA Z-scan and 0.07 mM by 2PF techniques. The good agreement between δ_{2PA} measured at low and high concentrations, as shown in Fig. 6, further confirms the negligible contribution from aggregates on 2PA in ACN solution in the spanned concentration range. As already observed in DCM, also in ACN the 2PA spectrum shows two main peaks and possibly a third one; however, their intensities differ from the vibronic peaks in DCM and the maximum δ_{2PA} value is about 2 times smaller.

The linear absorption spectrum of JB17-08 in ACN, measured at very low concentration (6.6 μM, where no aggregation can occur) shown in Fig. 7, points to the dynamical co-existence in solution of the symmetric and asymmetric forms of the molecule, in agreement with results obtained for other dyes undergoing symmetry breaking in the ground state.[11,17] Although it is physically impossible to isolate the asymmetric form from the symmetric one, we can *virtually* separate the contributions of these two forms to the linear absorption spectrum, as presented in Fig. 7. The black curve (1 in Fig. 7) shows the total linear absorption spectrum of JB17-08 in ACN. The contribution to the absorption spectrum given by the molecules in the symmetric form can be estimated from the absorption spectrum of the monomer in DCM – where we know that the symmetry is mainly preserved – after an appropriate shift (about 20 nm) to the blue: the result is represented by the blue shaded area in Fig. 7. The close overlap of these two absorption contours on the red side of the spectrum indicates that the absorption feature in ACN centered at 1043 nm is mainly due to the contribution from the symmetric form. We can extract the absorption spectrum of the asymmetric form by subtracting the contribution of the symmetric form (blue shaded area) from the total absorption profile (black curve 1). This contribution, dominating the blue side of the total spectrum, is shown as the red shaded area (under curve 3) in Fig. 7. As a result of this deconvolution, the concentration of the symmetric form in ACN can be estimated as ~42% of total dye concentration, corresponding to the ratio of peak molar absorptivities between ACN and DCM, and the concentration percentage of the asymmetric form can be estimated as ~58%.

Two leading factors are responsible for the 2PA band observed in ACN and shown in Fig. 6. As discussed above, the 2PA intensity of the symmetric form is vibronic in origin. In the asymmetric form, the lowered symmetry makes the 1PA transition allowed in 2PA due to the variation of the permanent dipole moment upon excitation, $\Delta\mu$. Quantum-chemical calculations, performed for the asymmetric form by *ab initio* method RHF/6-31G** (in standard Gaussian 2003 program package), suggest a $\Delta\mu$ as large as 17 D, comparable with the ground-to-excited-state transition dipole moment μ_{01} = 18 D (estimated experimentally as described in Section 2.1).

2.3.2. Excited-state absorption (ESA) spectra: results and analysis. To gain information on the excited-state geometries of the symmetric and asymmetric forms, we measured the ESA spectra with excitation into the peaks of both forms using the femtosecond white-light-continuum (WLC) pump–probe technique described in ref. 25. The pump pulse is generated by an optical parametric generator/amplifier (OPG/OPA, Light Conversion Ltd. model TOPAS-C) excited by a regenerative Ti:Sapphire amplifier (Clark-MXR). A weak portion of the pump pulse is delayed and then focused into a 1 cm water cell to generate a weak WLC probe pulse. Two identical narrow bandpass filters are used: one is placed in front of the sample to select a single probe wavelength and block any stimulated emission,[3]

and the other is placed in front of the detector to block scattered pump light, thus improving the signal-to-noise ratio. The spot size of the probe beam is approximately 3 times smaller than that of the pump, with the angle between pump and probe $\sim 5^\circ$ to make sure that the probe pulse is traveling through a homogeneously pumped solution area. The pump is also modulated at 285 Hz by a mechanical optical chopper synchronized with the repetition rate of the pump laser. A lock-in amplifier is used to record the signal. The ESA cross section, $\sigma_{1n}(\lambda)$ for each probe wavelength λ, is calculated using the following equation:[25]

$$\sigma_{1n}(\lambda) = \sigma_{01}(\lambda) - [\sigma_{01}(\lambda_{ESA}) - \sigma_{1n}(\lambda_{ESA})] \times \frac{\ln\left[T_{NL}(\lambda)/T_L(\lambda)\right]}{\ln\left[T_{NL}(\lambda_{ESA})/T_L(\lambda_{ESA})\right]} \quad (6)$$

where σ_{01} is the ground-state absorption cross section; T_L is the linear transmittance of the probe before the pump beam arrives at the sample; T_{NL} is the transmittance of the probe in the presence of the pump (after ~ 1 ps delay); $\lambda_{ESA} = 600$ nm (chosen close to the ESA peak) is the wavelength where σ_{1n} is measured independently by picosecond Z-scan. To build a significant population in the first excited state, the pump wavelength is set at the 1PA peak (peak of absorption of the symmetric form) in both DCM and ACN solutions. In ACN solution, where JB17-08 shows the strongest symmetry-breaking effect, another ESA spectrum was measured by pumping at 900 nm, *i.e.* in the peak of the absorption corresponding to the asymmetric form (see Fig. 7).

To obtain quantitative values for the ESA cross section, $\sigma_{1n}(\lambda)$, additional independent measurements at 600 nm (corresponding to the ESA peak) were performed using a picosecond pump pulse generated by an optical parametric generator/amplifier (OPG/OPA, EKSPLA, Model PG401 DFG) pumped by 10 Hz mode-locked Nd:YAG laser (EKSPLA, model PL2143, operating at 1064 nm with a 10 Hz repetition rate which is frequency tripled to pump the OPG/OPA). The pulsewidth is 13 ps (FWHM) measured independently by second-harmonic autocorrelation. A reference material, CS_2,[26] is used *via* closed-aperture Z-scan to calibrate the spot size (12.25 μm, HW1/e^2 M) of the focus and verify the pulsewidth of the Z-scan setup. For each sample, Z-scan measurements are performed with several different input energies, and the fitting is based on a three-level model using the rate and propagation equations shown below:

$$\begin{aligned} \frac{dI}{dz} &= -\sigma_{01}N_0 I - \sigma_{1n}N_1 I \\ \frac{dN_0}{dt} &= -\frac{\sigma_{01}N_0 I}{\hbar\omega} + \frac{N_1}{\tau_F} \\ \frac{dN_1}{dt} &= \frac{\sigma_{01}N_0 I}{\hbar\omega} - \frac{N_1}{\tau_F} - \frac{\sigma_{1n}N_1 I}{\hbar\omega} + \frac{N_n}{\tau_{n1}} \\ \frac{dN_n}{dt} &= \frac{\sigma_{1n}N_1 I}{\hbar\omega} - \frac{N_n}{\tau_{n1}} \end{aligned} \quad (7)$$

where I is the irradiance of the input pulse (Fresnel reflections included) as a function of the penetration depth z; τ_F and τ_{n1} are the lifetimes of the *first* and *higher* lying excited states; N_0, N_1, N_n are the population densities of the ground, first excited and higher-lying excited states, respectively. The fitting for different energies yields a single set of parameters: $\sigma_{1n} = (80 \pm 10) \times 10^{-17}$ cm^2, which is ~ 25 times larger than the ground-state cross section ($\sigma_{01} = 3.2 \times 10^{-17}$ cm^2), and $\tau_{n1} = 5 \pm 1$ ps. The ESA spectra and Z-scan traces of JB17-08 in ACN are shown in Fig. 8a and b. Note that JB17-08 in DCM solution shows similar ESA spectra.

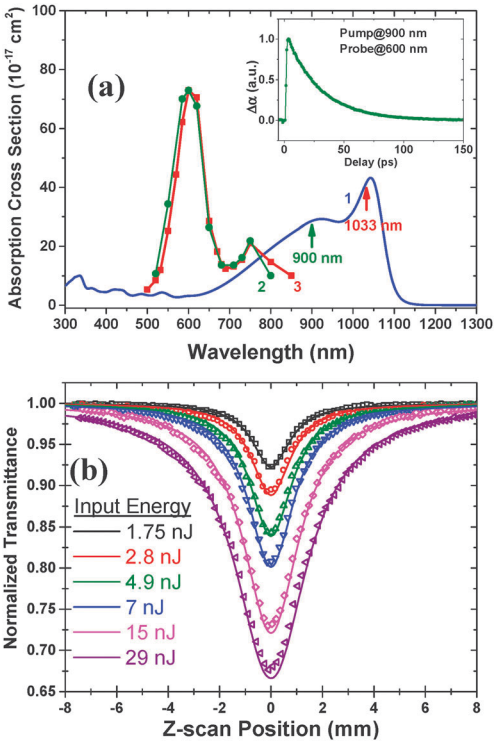

Fig. 8 JB17-08 in ACN: (a) linear absorption (1) and ESA spectra with excitation into the peak of the asymmetric form, 900 nm (green circles, 2) and with excitation into the peak of the symmetric form, 1033 nm (red squares, 3). The inset shows decay of the first excited state: $\tau_F = 28 \pm 2$ ps using a pump–probe experiment; (b) picosecond Z-scan traces (concentration 0.19 mM, 1 mm cell) at 600 nm with different input energies and corresponding fittings.

Fig. 8a shows ESA spectra measured in ACN solution upon excitation at the maximum of the absorption of the asymmetric form (curve 2) and at the maximum of the absorption of the symmetric form (curve 3). These two curves are practically coincident, confirming that the same *relaxed* excited-state geometry is reached after excitation of either the symmetric or asymmetric form.

3. Theoretical modeling

The extensive set of experimental data collected for JB17-08 invites a detailed theoretical analysis. Three-state model proved successful to rationalize symmetry breaking of long polymethine dyes dissolved in polar solvents and allowed their low-energy spectral features to be quantitatively reproduced in terms of a minimal set of adjustable model parameters.[11] The main resonance structures for JB17-08 can be schematically represented as D^+–π–D ↔ D–π^+–D ↔ D–π–D^+, where D stands

for the terminal donor groups and π for the polymethine chain. These three structures, labeled as Z_1, N and Z_2, respectively, are chosen as basis states in an essential-state approach. The two degenerate states Z_1 and Z_2 are separated by an energy gap 2η from state N, and the resonance integral $\tau = \langle Z_1|H_{el}|N\rangle = \langle Z_2|H_{el}|N\rangle$ (where H_{el} is the electronic Hamiltonian) mixes Z_1 and Z_2 with N. Symmetry-adapted basis states are conveniently introduced as N, $Z_+ = (Z_1 + Z_2)/\sqrt{2}$ and $Z_- = (Z_1 - Z_2)/\sqrt{2}$. In this basis the electronic Hamiltonian reads:

$$H_{el} = \begin{pmatrix} 0 & -\sqrt{2}\tau & 0 \\ -\sqrt{2}\tau & 2\eta & 0 \\ 0 & 0 & 2\eta \end{pmatrix} \quad (8)$$

H_{el} describes the coupling of the two totally-symmetric basis states, N and Z_+, to give the ground state $|g\rangle = \sqrt{1-\rho}|N\rangle + \sqrt{\rho}|Z_+\rangle$ and a totally-symmetric excited state $|e\rangle = \sqrt{1-\rho}|Z_+\rangle - \sqrt{\rho}|N\rangle$, where ρ, the weight of Z_+ in the ground state, represents the degree of symmetric quadrupolar charge separation in the ground state. The third antisymmetric state, $|c\rangle = |Z_-\rangle$, stays unmixed. Note, that the $|e\rangle$ state is higher in energy than the $|c\rangle$ state. Explicit expressions for ρ and for the energies of these three electronic states as functions of η and τ are given in ref. 16.

Z_1 and Z_2 have a large dipole moment of equal magnitude, μ_0, and opposite direction. Accordingly, the only non-negligible matrix elements of the dipole moment operator in the symmetry-adapted basis are: $\mu_0 = \langle Z_+|\hat{\mu}|Z_-\rangle = \langle Z_-|\hat{\mu}|Z_+\rangle$. The lowest-energy g → c transition (corresponding to $S_0 \rightarrow S_1$) is one-photon allowed, with $\mu_{gc} = \mu_0\sqrt{\rho}$, but is 2PA forbidden. The higher-energy transition g → e ($S_0 \rightarrow S_n$) is allowed in 2PA, even if it is experimentally eclipsed because of the proximity with the 1PA resonance. The c → e transition ($S_1 \rightarrow S_n$) is an ESA transition with a transition dipole moment $\mu_{ce} = \mu_0\sqrt{1-\rho}$.

This electronic model captures the main features of the optical spectra of polymethine dyes, but cannot describe the subtle dependence of band-shapes on solvent polarity and the sizable 2PA intensity in the region of the nominally 2PA-forbidden g → c transition. We therefore introduce a coupling of electronic states to molecular vibrations and polar solvation. Two effective molecular coordinates, Q_+ and Q_-, are introduced to account for the relaxation of the molecular geometry upon excitation. These two coordinates have harmonic frequencies $\omega_\pm$, and relaxation energies $\varepsilon_\pm$. Finally, polar solvation is described by the reaction electric field, F_{or}, generated at the solute location by the reorientation of polar solvent molecules around the solute.

The total Hamiltonian H reads:

$$H = \begin{pmatrix} 0 & -\sqrt{2}\tau & 0 \\ -\sqrt{2}\tau & 2\eta - \sqrt{\varepsilon_+}\omega_+ Q_+ & -\sqrt{\varepsilon_-}\omega_- Q_- - \mu_0 F_{or} \\ 0 & -\sqrt{\varepsilon_-}\omega_- Q_- - \mu_0 F_{or} & 2\eta - \sqrt{\varepsilon_+}\omega_+ Q_+ \end{pmatrix} + \frac{P_+^2 + \omega_+^2 Q_+^2}{2} + \frac{P_-^2 + \omega_-^2 Q_-^2}{2} + \frac{\mu_0^2 F_{or}^2}{4\varepsilon_{or}} \quad (9)$$

where the first term is the electronic Hamiltonian H_{el} in eqn (8), but with relevant energies modulated by the two vibrational coordinates Q_+ and Q_- and by the reaction field F_{or}. The second and third terms are the harmonic oscillator Hamiltonians relevant to Q_+ and Q_- (P_+ and P_- are the conjugate momenta), and the last term is the elastic energy associated with the reaction field.

The dynamics of F_{or} is governed by the slow rotation of solvent molecules. F_{or} can then be treated as a classical variable and the Hamiltonian H in eqn (9) can be solved on a grid of F_{or} values. For each F_{or} value, the Hamiltonian describes both electronic and vibrational degrees of freedom, and we propose a numerical *non-adiabatic* solution. Specifically, a non-adiabatic basis set is defined as the direct product of the three electronic basis states, multiplied by the eigenstates of the two harmonic oscillators described by the second and third term of the Hamiltonian in eqn (9). For numerical purposes, the infinite basis associated with each one of the two harmonic oscillators is truncated to a finite number (M), leading to an overall dimension $3M^2$ for the non-adiabatic basis. The matrix elements of the F_{or}-dependent Hamiltonian are readily written in this basis, and the corresponding matrix can be numerically diagonalized to get the vibronic eigenstates of the system. The solution is numerically exact provided M is large enough to ensure convergence (in this paper we set $M = 10$). The F_{or}-dependent vibronic eigenstates enter the expressions for optical spectra, as explicitly discussed in ref. 27. In the calculation of optical spectra, a fixed intrinsic bandwidth 2Γ (FWHM) is assigned to each eigenstate (corresponding to a width $\sigma = \Gamma/\sqrt{2\ln 2}$ in the case of Gaussian bandshapes). Spectra in solution are finally obtained as thermal averages of spectra calculated for different F_{or} values. Specifically, 1PA and 2PA spectra are averaged assuming a Boltzmann distribution based on the F_{or}-dependent ground-state energy, while fluorescence and ESA spectra are averaged over the Boltzmann distribution related to the excited state.

The spectra, shown in Fig. 9 are calculated with optimized model parameters shown in Table 1. All molecular parameters, including the electronic parameters, η, τ and μ_0, the vibrational frequencies $\omega_\pm$, relaxation energies $\varepsilon_\pm$ and the intrinsic bandwidth Γ, are strictly solvent-independent. Only the solvent relaxation energy, ε_{or}, is tuned to account for increasing solvent polarity from DCM to ACN. The value assigned to μ_0 (24.5 D) corresponds to a distance of ~5 Å between each lateral donor group and the center of the π-bridge, amounting to a distance between the two lateral donor groups of ~10 Å. This value is somewhat underestimated with respect to the actual distance, in line with the discussion in ref. 28. The frequency and coupling constants assigned to the two effective vibrational modes were selected to reproduce the vibronic profile of absorption and emission spectra. These effective modes cannot be simply identified with specific molecular vibrational modes as seen in IR and/or Raman spectroscopy.[29] However, the two effective frequencies, amounting to 1050 and 1450 cm^{-1} and the corresponding coupling constants are consistent with typical vibrational frequencies of polyacetylene.[30] The solvent

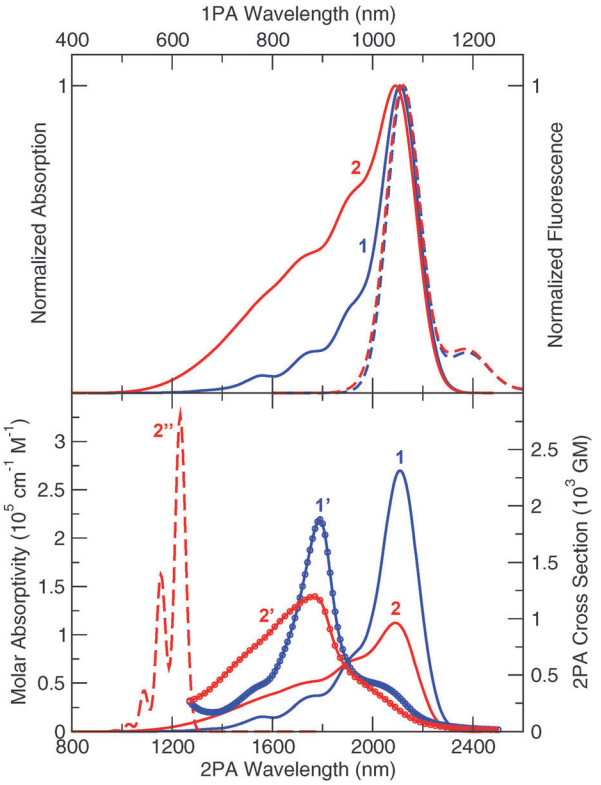

Fig. 9 Calculated spectra according to the essential-state model using model parameters reported in Table 1 (blue lines: low-polarity solvent; red lines: high-polarity solvent). Top panel: normalized 1PA (full lines 1 and 2) and fluorescence (dashed lines) spectra. Bottom panel: 1PA (full lines 1 and 2), 2PA (circles 1′ and 2′) and ESA (line 2″) spectra. Top axis is related to 1PA, fluorescence and ESA. Bottom axis is related to 2PA. The calculated ESA spectrum is the same in both solvents. The ESA peak corresponds to a cross section of 127 × 10^{-17} cm^2.

Table 1 Parameters of the three-state model for JB17-08

τ [eV]	η [eV]	ω_+ [eV]	ω_- [eV]	ε_+ [eV]	ε_- [eV]	ε_{or} [eV] (DCM/ACN)	Γ [eV]	μ_0 [D]
1.07	−0.32	0.13	0.18	0.37	0.45	0.23/0.35	0.04	24.5

relaxation energy, ε_{or}, can be easily related to solvent polarity indicators (in particular the solvent dielectric constant and refractive index, through the Δf function), at least in the approximation of a spherical cavity occupied by the solute inside the dielectric.[31] The values that we fixed for ε_{or} in the two solvents (DCM and ACN) scale well with the Δf function and correspond to a cavity diameter of ∼14 Å, well in line with the real molecular dimension.

Calculated spectra quantitatively reproduce experimental spectra, a non-trivial result in view of the modest number of adjustable model parameters and of the complex spectral behavior of JB17-08.

In previous models applied to polymethine dyes,[11] the same vibrational frequency and relaxation energy were assigned to Q_+ and Q_-. Here, for the first time, we have access to 2PA spectra of a polymethine dye dissolved in a low polarity solvent like DCM. These spectra show a partly resolved vibronic structure. In these conditions, a reasonable simultaneous fit of 1PA and 2PA band-structures in DCM enforced the use of a slightly more elaborate model. In fact, both linear and 2PA spectra in DCM solution are mainly due to the symmetric form of the dye. In these conditions, 1PA spectra are dominated by Q_+, the totally-symmetric mode responsible for the vibronic progression, while 2PA spectra are dominated by Q_-, the antisymmetric vibration responsible for the vibronic activation of the nominally forbidden 2PA band.

4. Discussion

We are now in a position to understand, in a unifying and internally consistent picture, optical spectra of JB17-08, including 1PA, 2PA, fluorescence and ESA, and their non-trivial dependence on solvent polarity. As discussed in the experimental section, optical spectra have contributions from both the symmetric and asymmetric forms of the dye, with the asymmetric form contribution increasing with solvent polarity. Fig. 10 shows the ground-state energy calculated with the model parameters in Table 1, as a function of the solvation reaction field F_{or}. The top and middle panels refer to ε_{or} = 0.23 and 0.35 eV, optimized to reproduce the observed spectra in DCM and ACN solutions, respectively. In DCM the ground-state energy shows a single minimum at F_{or} = 0, corresponding to the symmetric form. In ACN, instead, the double-minimum structure points to a broken-symmetry ground state: the energy minimum is not found at F_{or} = 0 (symmetric form), but at finite (equal and opposite) F_{or} values, corresponding to the two (equivalent) asymmetric forms.

In the hypothetical zero-temperature limit, only the equilibrium configuration would be populated, and all the molecules in solution would experience the same reaction field, corresponding to the minimum/minima of the ground-state energy. According to Fig. 10a, in this zero-temperature limit, all the chromophore molecules dissolved in DCM would be in the symmetric form (energy minimum at F_{or} = 0). The relevant 1PA and 2PA spectra calculated for F_{or} = 0 are reported in Fig. 10c, and show non-coincident spectral positions. Indeed, for the symmetric molecule, optical selection rules are different for 1PA and 2PA processes, and different states contribute to the two processes. 1PA spectra of the pure symmetric form (Fig. 10) are largely dominated by the 0–0 transition and the 0–0, 0–1_+, 0–2_+, *etc.* progression is clearly seen, associated to excited vibrational states of the symmetric Q_+ mode. All of these transitions are strictly forbidden in 2PA, which is instead associated with a transition into the same electronic state but with different vibrational modes, *i.e.* the asymmetric vibrational mode. Specifically the 0–1_- transition, is clearly seen in the spectrum, while 0–2 is forbidden and 0–3 is most probably too weak to be recognized. The 2PA intensity is therefore vibronic in origin, being driven by the coupling to the antisymmetric vibrational mode.

In the same zero-temperature limit, in ACN solution, all molecules would be located in either one of the two minima shown in Fig. 10b (of course, molecules experiencing equal and opposite F_{or} are strictly equivalent), corresponding to an

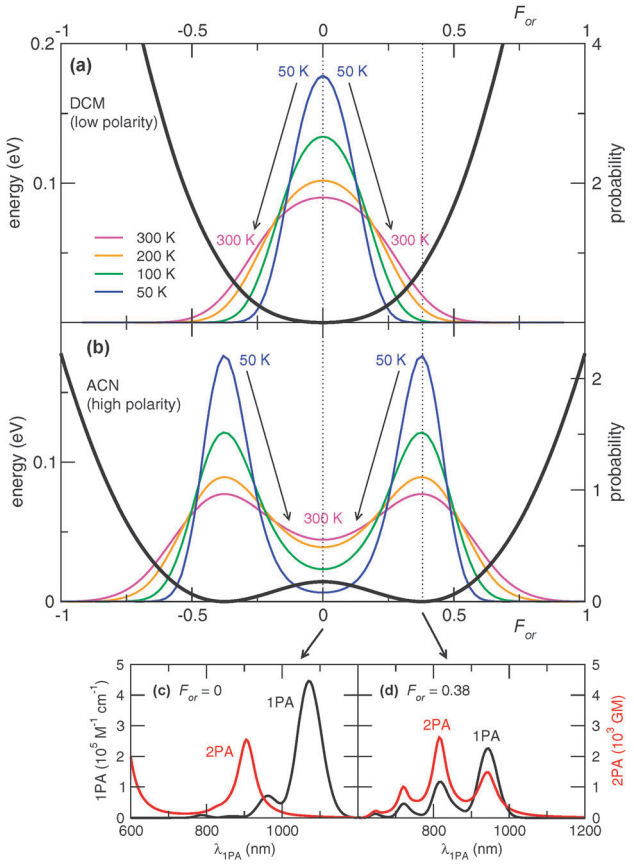

Fig. 10 Top: parts (a) and (b): calculated ground-state energy (black thick line) *vs.* the solvation reaction field F_{or} for the low-polarity solvent (a, ε_{or} = 0.23 eV modeling DCM) and for the high-polarity solvent (b, ε_{or} = 0.35 eV modeling ACN); Boltzmann probability distributions of the reaction field (based on the ground-state energy) at different temperatures (see legend). Bottom: 1PA (black) and 2PA (red) spectra calculated for (c) F_{or} = 0, and (d) for the F_{or} value corresponding to the energy minima of (b).

asymmetric form. 1PA and 2PA spectra calculated in this hypothetical limit are shown in Fig. 10d. 1PA spectra show a well-resolved vibronic structure with maximum intensity for the 0–0 transition. But now, since the molecule is in an asymmetric form, the same states responsible for 1PA are also 2PA-active. However, the relative intensities of the vibronic bands are markedly different in 1PA and 2PA, with the 2PA maximizing at the 0–1_+ transition. This result, obtained here with the three-state model for polymethine dyes, is in line with the results of a simpler two-state model applied to polar molecules.[24]

According to ref. 16, quadrupolar dyes can be classified into three different families with distinctively different spectroscopic behaviors. Class I dyes, characterized by low quadrupolar charge separation, undergo symmetry breaking in the first excited state (with important solvatochromic effects on emission bands). Class II chromophores, characterized by intermediate quadrupolar charge separation, are not prone to symmetry breaking: their ground and excited states maintain a symmetric charge distribution, and their optical spectra are only marginally affected by solvent polarity. Chromophores with very high quadrupolar charge separation belong to class III, and undergo symmetry breaking in the ground state, with important solvation effects on absorption spectra. As demonstrated in ref. 11, long PDs are representatives of class III chromophores, at least in high-polarity solvents. Results reported here for JB17-08 confirm that symmetry breaking in the ground state of class III dyes is favored in polar solvents.

At finite temperature, due to thermal disorder, the solution can be described as a collection of solute molecules being surrounded by a different configuration of solvent molecules, *i.e.* experiencing different F_{or}. In these conditions, a *continuous* distribution of the reaction field is calculated according to the Boltzmann law, as shown in Fig. 10a and b for DCM and ACN solutions, respectively, for a few selected temperatures. Solution spectra at finite temperature are calculated as the weighted sum of spectra relevant to different F_{or}. Since the spectra depend on F_{or} (see Fig. 10c and d), important inhomogeneous broadening effects are expected with increasing temperature.

The temperature evolution of calculated 1PA and 2PA spectra is shown in Fig. 11. In DCM, temperature effects are minor: indeed, the distribution is always dominated by the symmetric form, so that the broadening of the distribution at finite temperature just results in spectral broadening. The minor

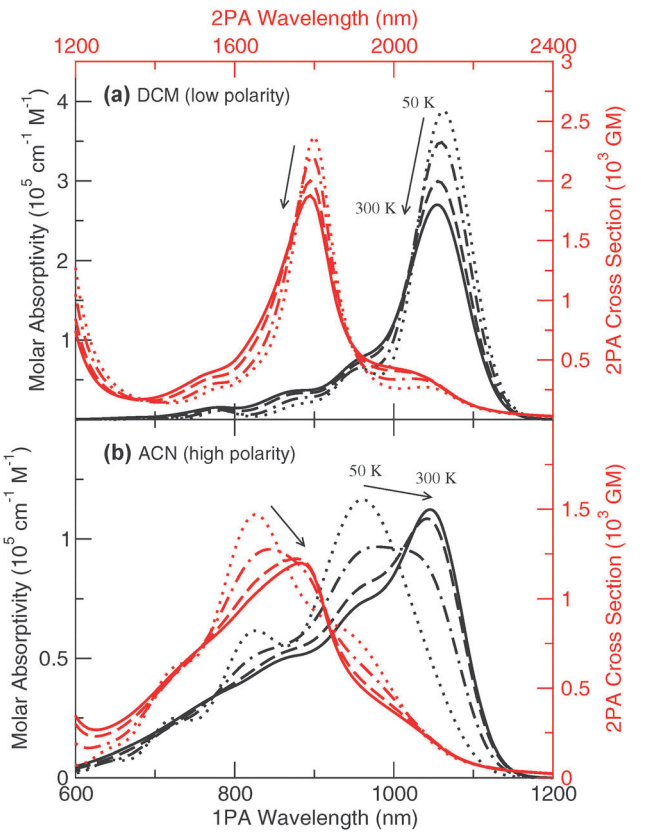

Fig. 11 1PA spectra (black lines) and 2PA spectra (red lines) calculated at T = 50, 100, 200 and 300 K (in the order indicated by the arrows: dots for 50 K, dash-dots for 100 K, dash for 200 K and solid lines for 300 K) in DCM (a, ε_{or} = 0.23 eV,) and ACN (b, ε_{or} = 0.35 eV). Note how for the higher-polarity solvent the spectra are much broader and have a different shape. This is due to symmetry breaking, as explained in Fig. 10 and 12.

increase of the 2PA intensity on the blue-side of the spectrum is due to a slight increase of the population of molecules experiencing a sizable F_{or}, and hence showing a slight asymmetry. The case of ACN solutions is more interesting. At very low temperature the population of the symmetric form (corresponding to $F_{or} = 0$) is negligible, but it increases with temperature. As a result, the temperature evolution of the calculated 1PA and 2PA spectra, shown in Fig. 11b, is far from trivial: not only inhomogeneous broadening increases with temperature, but signatures of the symmetric form become more and more evident, leading to an overall red shift of the 1PA band. The concomitant evolution of the 2PA band is even more involved, resulting from the very complex evolution of the 2PA band with F_{or} (see Fig. 10c and d). In any case, the 2PA intensity is not expected to be significantly increased upon a temperature increase.

Fluorescence spectra are not affected by solvent polarity, and do not show features related to the asymmetric form. To clarify this point, Fig. 12 shows the energies of the ground state, of the first excited state (responsible for fluorescence and ESA), and of the higher-lying excited state (reached by ESA), calculated as a function of F_{or} for model parameters relevant to ACN solutions. As discussed above, in this solvent the ground-state energy shows a double minimum as a function of F_{or}, so that at room temperature a sizable population is expected for the symmetric and asymmetric forms of the dye. On the contrary, the energy of the fluorescent state *versus* F_{or} shows a single minimum, so that the Boltzmann distribution relevant to the fluorescent state has a single narrow maximum located at $F_{or} = 0$. Thus, fluorescence and ESA processes, both starting from the fluorescent state, are always dominated by the symmetric form of the dye, irrespectively of solvent polarity. From Fig. 12 we can understand why the absorption due to the asymmetric form is always located to the blue of the absorption related to the symmetric form: the first one involves a process starting from one of the two equivalent minima in the ground state, while the second one involves the vertical excitation at $F_{or} = 0$, *i.e.* starting from the relative maximum in the ground-state potential energy surface.

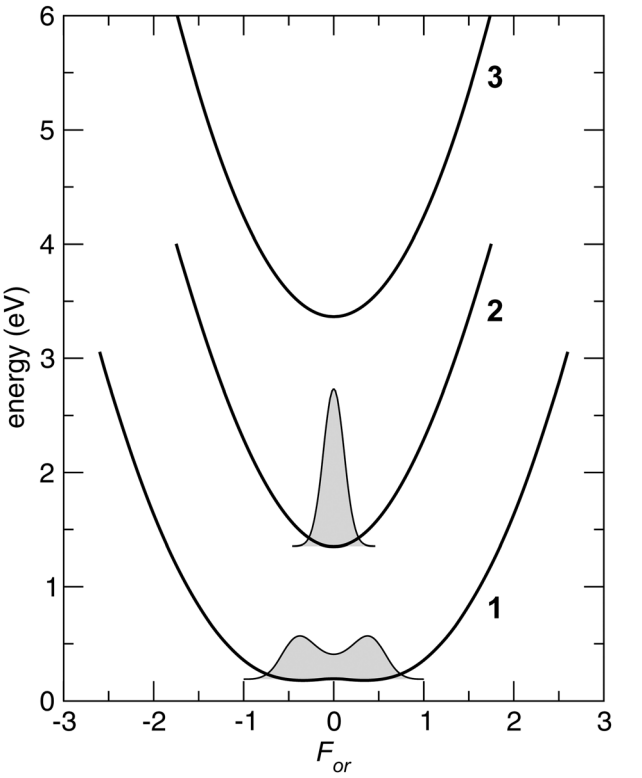

Fig. 12 Calculated energies of the ground state (1), fluorescent (first excited) state (2) and the higher-lying excited state (3), *vs.* the solvation reaction field F_{or}, for ε_{or} = 0.35 eV (ACN). The shadowed areas represent the probability distributions of the reaction field calculated according to the Boltzmann law using the ground state (1) or the first excited state (2) energies.

5. Conclusions

We presented an extensive experimental study and a detailed theoretical analysis of the spectroscopic properties of the cationic polymethine 2-azaazulene dye, JB17-08. This dye undergoes symmetry breaking in polar solvents in spite of having a comparatively short polymethine chain (n = 3). The electronic transitions of JB17-08 are located in the NIR region, making experimental measurements, and particularly the collection of 2PA spectra, a non-trivial task. We were able to collect linear (absorption, fluorescence and excitation anisotropy) and nonlinear (2PA and ESA) spectra of JB17-08 in two solvents (DCM and ACN) with distinctively different polarities. Since nonlinear measurements require comparatively concentrated solutions (typically $\geq 10^{-3}$ M) with respect to linear measurements (typically 10^{-5}–10^{-6} M), aggregation in low-polarity solvents (here in DCM) hinders the collection of nonlinear spectra for polymethine dyes. Indeed, the 2PA spectrum reported here for JB17-08 in DCM represents the nonlinear spectrum of a cationic polymethine dye collected in one of the lowest polarity environments. The experimental efforts spent to obtain reliable 2PA data for JB17-08 in DCM were motivated by the possibility of comparing spectra obtained in a solvent where JB17-08 does not undergo symmetry breaking (such as DCM), with spectra measured in polar solvents (such as ACN), where JB17-08 is preferentially in a broken-symmetry ground state. The distinctively different 2PA spectra collected in the two solvents offered an intriguing interpretative challenge.

High-quality first-principle quantum chemical calculations, providing a description of electronic states in polymethine dyes and their evolution with solvent polarity, are still in their infancy[32–36] and, to the best of our knowledge, have not yet been applied to 2PA and ESA in systems undergoing symmetry breaking. Here we propose a different approach, aimed at the understanding of the *essential* physics and chemistry of such complex systems. Therefore, we based our analysis on phenomenological essential-state models that, adopting a minimal basis set to describe the electronic structure, explicitly introduce the coupling of electronic degrees of freedom to molecular vibrations and to an effective solvation coordinate. Essential-state models are semiempirical in nature, since model parameters must be fixed against experimental data. They are not based on a molecular orbital description and in this sense they have an intrinsic

many-body nature. The selected essential states are diabatic states and cannot be identified with the first few states out of the complete set of excited states obtained through a first-principle calculation. We adopt a semiempirical approach, extracting essential states based on chemical intuition (the valence bond picture) and parameterize the model against experiment. This approach has already been successfully applied to describe linear and nonlinear optical properties of several families of organic dyes.[11,16,27,28,37–43] Recently Olsen and McKenzie have devised a computationally expensive but rigorous procedure to extract essential-state models from high-quality *ab initio* calculations, demonstrating their intrinsically many-body nature.[44–48]

In particular, essential-state models allow the calculation of linear and nonlinear optical spectra of target organic chromophores based on a handful of empirical molecular parameters that are strictly solvent-independent, being relevant to the basis states, *i.e.* to the main resonating structures of the molecule at hand. The solvent dependence of the calculated spectra are therefore not forced in the model by tuning molecular parameters, as done, *e.g.*, in the well-known Mulliken–Hush model for polar dyes,[49–51] but results naturally from the dependence of the eigenstates of the system on the solvent polarity. The solvent polarity itself enters the model with a single adjustable parameter, the solvent relaxation energy relevant to basis states.

Essential-state models have already been successfully exploited for two families of polymethine dyes.[11] Here the same model has been adopted for JB17-08. The large amount of experimental data available for this dye allowed us to safely parameterize the model: we stress that all spectra, including linear absorption and fluorescence, ESA and 2PA in both solvents, are calculated based on just the 10 adjustable model parameters shown in Table 1. This number of adjustable parameters may seem large at first sight, but a (low-quality) fit of just the absorption spectrum in a single solvent would require a minimum of 6 adjustable parameters (to locate the position, intensity and width of the two main features observed in 1PA). Similarly, a numerical fit of just one of the 2PA bands would require at least an additional set of 6 adjustable parameters. Within our approach, we reproduce *at the same time* 1PA, 2PA, ESA and fluorescence spectra collected in two different solvents with a grand total of 10 model parameters. This would definitely be impossible without a reliable microscopic model. The distinctively different bandshapes observed for 1PA, fluorescence and 2PA spectra are not obtained by readjusting an effective bandwidth assigned to each process: in our model the intrinsic width associated to each transition is assigned the same value, Γ, for all processes, independent of the solvent polarity. The evolution of the bandshapes turns out naturally from the adopted model that accounts for the thermal disorder associated with polar solvation and for its distinctively different effects on the ground and excited molecular states. The very good agreement between experimental and calculated spectra then gives confidence on the reliability of the proposed model as a powerful interpretative tool for optical spectra of polymethine dyes in solutions.

On this basis, we are able to explain the complex dependence on solvent polarity of the 2PA spectra of JB18-07. Due to thermal disorder in solution, the overall spectra represent the superposition of spectra relevant to molecules experiencing different reaction fields. The contribution from dyes in the symmetric form, corresponding to molecules experiencing negligible values of F_{or}, dominates spectra collected in DCM, while the contribution from asymmetric forms, related to molecules experiencing a sizable reaction field, dominates in ACN. The 2PA band of the symmetric form is purely vibronic in origin and appears near to the 0–1 transition of the 1PA spectrum (the two peaks are not coincident due to the small frequency difference between the symmetric vibration responsible for the 1PA progression and the antisymmetric vibration responsible for the 2PA intensity). 2PA becomes allowed into the same states responsible for 1PA for dyes in the asymmetric form, so that coincident 1PA and 2PA transitions are expected. However, as originally predicted in ref. 24, the vibronic structures associated with 1PA and 2PA transitions can be very different, with the 2PA intensity generally shifted to higher energies with respect to the 1PA band.

The solvent dependence of 2PA spectra of polymethine dyes undergoing symmetry breaking is therefore difficult to predict based on simple intuitive concepts. It results from a subtle balance between a vibronic contribution, dominating for dyes in the symmetric form, and hence in low-polarity solvents, and a contribution from the asymmetric form, dominating in high-polarity solvents. The prevalence of one contribution or the other depends on the relative strength of the electron-vibration coupling and of solvent polarity in a complex interplay that requires detailed interpretative models.

Acknowledgements

This work is supported by ARO 50372-CH-MUR, DARPA ZOE W31R4Q-09-1-0012, and AFOSR MURI FA9550-10-1-0558. F.T. thanks Fondazione Cariparma for financial support and MIUR (Italian Ministry of University and Research) for funding through the Project FIRB-Futuro in Ricerca RBFR10Y5VW.

References

1 M. Pawlicki, H. A. Collins, R. G. Denning and H. L. Anderson, *Angew. Chem., Int. Ed.*, 2009, **48**, 3244–3266.
2 O. V. Przhonska, S. Webster, L. A. Padilha, H. Hu, A. D. Kachkovski, D. J. Hagan and E. W. Van Stryland, in *Advanced Fluorescence Reporters in Chemistry and Biology I: Fundamentals and Molecular Design, Springer Series in Fluorescence*, ed. A. P. Demchenko, Springer-Verlag, Berlin, Heidelberg, 2010.
3 L. A. Padilha, S. Webster, H. Hu, O. V. Przhonska, D. J. Hagan, E. W. Van Stryland, M. V. Bondar, I. G. Davydenko, Y. L. Slominsky and A. D. Kachkovski, *Chem. Phys.*, 2008, **352**, 97–105.
4 J. M. Hales, J. Matichak, S. Barlow, S. Ohira, K. Yesudas, J.-L. Brédas, J. W. Perry and S. R. Marder, *Science*, 2010, **327**, 1485–1488.
5 S. Mukhopadhyay, C. Risko, S. R. Marder and J.-L. Bredas, *Chem. Sci.*, 2012, **3**, 3103–3112.

6 Z. Li, Y. Liu, H. Kim, J. M. Hales, S.-H. Jang, J. Luo, T. Baehr-Jones, M. Hochberg, S. R. Marder, J. W. Perry and A. K. Y. Jen, *Adv. Mater.*, 2012, **24**, OP326–OP330.
7 J. D. Matichak, J. M. Hales, S. Ohira, S. Barlow, S.-H. Jang, A. K. Y. Jen, J.-L. Brédas, J. W. Perry and S. R. Marder, *ChemPhysChem*, 2010, **11**, 130–138.
8 M. Rumi, J. E. Ehrlich, A. A. Heikal, J. W. Perry, S. Barlow, Z. Hu, D. McCord-Maughon, T. C. Parker, H. Röckel, S. Thayumanavan, S. R. Marder, D. Beljonne and J.-L. Brédas, *J. Am. Chem. Soc.*, 2000, **122**, 9500–9510.
9 J. Fu, L. A. Padilha, D. J. Hagan, E. W. Van Stryland, O. V. Przhonska, M. V. Bondar, Y. L. Slominsky and A. D. Kachkovski, *J. Opt. Soc. Am. B*, 2007, **24**, 56.
10 S. Ohira, I. Rudra, K. Schmidt, S. Barlow, S.-J. Chung, Q. Zhang, J. Matichak, S. R. Marder and J.-L. Brédas, *Chem.–Eur. J.*, 2008, **14**, 11082–11091.
11 F. Terenziani, O. V. Przhonska, S. Webster, L. A. Padilha, Y. L. Slominsky, I. G. Davydenko, A. O. Gerasov, Y. P. Kovtun, M. P. Shandura, A. D. Kachkovski, D. J. Hagan, E. W. Van Stryland and A. Painelli, *J. Phys. Chem. Lett.*, 2010, **1**, 1800–1804.
12 R. S. Lepkowicz, O. V. Przhonska, J. M. Hales, J. Fu, D. J. Hagan, E. W. Van Stryland, M. V. Bondar, Y. L. Slominsky and A. D. Kachkovski, *Chem. Phys.*, 2004, **305**, 259.
13 J. R. Lakowicz, *Principle of Fluorescence Spectroscopy*, Kluwer Academic/Plenum Publisher, New York, 2nd edn, 1999.
14 O. V. Przhonska, H. Hu, S. Webster, J. L. Bricks, A. A. Viniychuk, A. D. Kachkovski and Y. L. Slominsky, *Chem. Phys.*, 2013, **411**, 17–25.
15 L. M. Tolbert and X. Zhao, *J. Am. Chem. Soc.*, 1997, **119**, 3253.
16 F. Terenziani, A. Painelli, C. Katan, M. Charlot and M. Blanchard-Desce, *J. Am. Chem. Soc.*, 2006, **128**, 15742–15755.
17 S. Webster, L. A. Padilha, H. Hu, O. V. Przhonska, D. J. Hagan, E. W. Van Stryland, M. V. Bondar, I. G. Davydenko, Y. L. Slominsky and A. D. Kachkovski, *J. Lumin.*, 2008, **128**, 1927.
18 O. V. Przhonska, D. J. Hagan, E. Novikov, R. Lepkowicz, E. W. Van Stryland, M. V. Bondar, Y. L. Slominsky and A. D. Kachkovski, *Chem. Phys.*, 2001, **273**, 235–248.
19 K. D. Belfield, M. V. Bondar, F. E. Hernandez, O. V. Przhonska and S. Yao, *Chem. Phys.*, 2006, **320**, 118–124.
20 F. Würthner, S. Yao, T. Debaerdemaeker and R. Wortmann, *J. Am. Chem. Soc.*, 2002, **124**, 9431–9447.
21 M. Sheik-Bahae, A. A. Said, T.-H. Wei, D. J. Hagan and E. W. Van Stryland, *IEEE J. Quantum Electron.*, 1990, **26**, 760–769.
22 W. C. Hurlbut, Y.-S. Lee, K. L. Vodopyanov, P. S. Kuo and M. M. Fejer, *Opt. Lett.*, 2007, **32**, 668–670.
23 M. R. Ferdinandus, M. Reichert, T. R. Ensley, H. Hu, D. A. Fishman, S. Webster, D. J. Hagan and E. W. Van Stryland, *Opt. Mater. Express*, 2012, **2**, 1776–1790.
24 A. Painelli, L. Del Freo and F. Terenziani, *Chem. Phys. Lett.*, 2001, **346**, 470–478.
25 R. A. Negres, O. V. Przhonska, D. J. Hagan, E. W. Van Stryland, M. V. Bondar, Y. L. Slominsky and A. D. Kachkovski, *IEEE J. Sel. Top. Quantum Electron.*, 2001, **7**, 849–863.
26 R. A. Ganeev, A. I. Ryasnyansky, M. Baba, M. Suzuki, N. Ishizawa, M. Turu, S. Sakakibara and H. Kuroda, *Appl. Phys. B: Lasers Opt.*, 2004, **78**, 433–438.
27 L. Grisanti, C. Sissa, F. Terenziani, A. Painelli, D. Roberto, F. Tessore, R. Ugo, S. Quici, I. Fortunati, E. Garbin, C. Ferrante and R. Bozio, *Phys. Chem. Chem. Phys.*, 2009, **11**, 9450–9457.
28 L. Grisanti, G. D'Avino, A. Painelli, J. Guasch, I. Ratera and J. Veciana, *J. Phys. Chem. B*, 2009, **113**, 4718–4725.
29 E. Ehrenfreund, C. C. Wu and Z. V. Vardeny, *Synth. Met.*, 2005, **155**, 266–269.
30 A. Girlando, A. Painelli and Z. G. Soos, *J. Chem. Phys.*, 1993, **98**, 7459–7465.
31 A. Painelli, *Chem. Phys.*, 1999, **245**, 185–197.
32 R. Improta, V. Barone and F. Santoro, *Angew. Chem., Int. Ed.*, 2007, **46**, 405–408.
33 V. Barone, R. Improta and N. Rega, *Acc. Chem. Res.*, 2008, **41**, 605–616.
34 V. Barone, J. Bloino, M. Biczysko and F. Santoro, *J. Chem. Theory Comput.*, 2009, **5**, 540–554.
35 N. Lin, Y. Luo, K. Ruud, X. Zhao, F. Santoro and A. Rizzo, *ChemPhysChem*, 2011, **12**, 3392–3403.
36 J. Fabian, *Dyes Pigm.*, 2010, **84**, 36.
37 F. Terenziani, A. Painelli and D. Comoretto, *J. Phys. Chem. A*, 2000, **104**, 11049–11054.
38 B. Boldrini, E. Cavalli, A. Painelli and F. Terenziani, *J. Phys. Chem. A*, 2002, **106**, 6286–6294.
39 F. Terenziani, A. Painelli, A. Girlando and R. M. Metzger, *J. Phys. Chem. B*, 2004, **108**, 10743–10750.
40 F. Terenziani, C. Sissa and A. Painelli, *J. Phys. Chem. B*, 2008, **112**, 5079–5087.
41 C. Sissa, V. Parthasarathy, D. Drouin-Kucma, M. H. V. Werts, M. Blanchard-Desce and F. Terenziani, *Phys. Chem. Chem. Phys.*, 2010, **12**, 11715–11727.
42 J. Campo, A. Painelli, F. Terenziani, T. Van Regemorter, D. Beljonne, E. Goovaerts and W. Wenseleers, *J. Am. Chem. Soc.*, 2010, **132**, 16467–16478.
43 C. Sissa, A. Painelli, M. Blanchard-Desce and F. Terenziani, *J. Phys. Chem. B*, 2011, **115**, 7009–7020.
44 S. Olsen and R. H. McKenzie, *J. Chem. Phys.*, 2009, **130**, 184302.
45 S. Olsen, *J. Chem. Theory Comput.*, 2010, **6**, 1089–1103.
46 S. Olsen and R. H. McKenzie, *J. Chem. Phys.*, 2011, **134**, 114520.
47 S. Olsen, *J. Phys. Chem. A*, 2012, **116**, 1486–1492.
48 S. Olsen and R. H. McKenzie, *J. Chem. Phys.*, 2012, **136**, 234313.
49 N. S. Hush, in *Prog. Inorg. Chem.*, ed. F. Albert Cotton, John Willey & Sons, New York, 1967, vol. 8, pp. 391–444.
50 N. S. Hush, *Coord. Chem. Rev.*, 1985, **64**, 135–157.
51 N. S. Hush and J. R. Reimers, *Chem. Rev.*, 2000, **100**, 775–786.

